INSTITUTE OF PHYSICS PUBLISHING JOURNAL OF PHYSICS B: ATOMIC, MOLECULAR AND OPTICAL PHYSICS

J. Phys. B: At. Mol. Opt. Phys. **34** (2001) 3073–3087 PII: S0953-4075(01)21526-0

Complete experiments for the double ionization of He: (e, 3e) cross sections at 1 keV impact energy and small momentum transfer

A Lahmam-Bennani[1,5], A Duguet[1], M N Gaboriaud[1], I Taouil[1], M Lecas[1], A Kheifets[2], J Berakdar[3] and C Dal Cappello[4]

[1] Laboratoire des Collisions Atomiques et Moléculaires (UMR 8625) Bât. 351, Université de Paris-Sud XI, F-91405 Orsay Cedex, France
[2] Research School of Physical Sciences, The Australian National University, Canberra ACT 0200, Australia
[3] Max-Planck Institut für Mikrostruktur Physik, Weinberg 2, D-06120 Halle, Germany
[4] Institut de Physique, LPMC, 1 Boulevard Arago, Technopôle 2000, F-57078 Metz, France

E-mail: azzedine@lcam.u-psud.fr

Received 29 January 2001, in final form 25 May 2001
Published 23 July 2001
Online at stacks.iop.org/JPhysB/34/3073

Abstract
The relative, coplanar angular distributions of electrons, produced in an electron-impact double ionization of helium (e, 3e reaction), have been measured at 1.1 keV impact energy. The momentum transfer was 0.45 au and the two 'ejected' electrons were detected with the same energy of 10 eV. The general features of the angular distributions are discussed. The data are analysed in different angular modes which allows a detailed comparison with state-of-the-art calculations. For high incident energy and small momentum transfer, as in the present case, the (e, 3e) cross section can be related to the single-photon double ionization (PDI). We exploit this fact and compare the present findings with the PDI and identify the contribution of non-dipole effects.

1. Introduction

The study of atomic electron-impact double ionization, also called the (e, 3e) reaction, provides a powerful and straightforward tool for investigating the dynamics of interacting, highly excited few-electron systems (three highly excited electrons in the field of a residual ion). A rather complete picture of the (e, 3e) process is obtained by performing an experiment in which the momentum vectors of all the particles are determined (a complete experiment would require resolving the spins as well). In the present experiment the reaction cross section is measured while the solid emission angles of the three electrons and the energies of two of them are

[5] Author to whom correspondence should be addressed.

determined, i.e. a fivefold differential cross sections (5DCS) is registered. Other kinematical variables of the involved particles are obtained from the energy and (linear) momentum conservation laws.

Recently, we conducted a systematic study of the (e, 3e) reaction employing various targets (Kr [1], Ar [2], Ne [3] and He [4–6]). Basically, all of these measurements have been carried out at a relatively high impact energy (~ 5.5 keV) and a small momentum transfer to the target. Therefore, the corresponding theoretical models [5–10] have been designed in the spirit of the first Born approximation (FBA) for the projectile–target interaction. Most of the theoretical results have been obtained using He as a target since the residual ion (the alpha particle) has no relevant internal structure, thus leading to a simplified theoretical treatment. The comparison of these theories with experiment has led to the following observations. The absolute magnitude of the calculated cross sections was largely different from one calculation to another and from the experimental absolute data. In general, however, the qualitative features of the measured angular correlation patterns at various fixed ejection angles were reproduced by the theories. In several cases the calculations deviated significantly from the experiments with regard to the shape of the angular correlation patterns. This disagreement was attributed, at least partly, to the non-first Born effects which were not included in most of the theoretical models (note that the C4FS model described in [5] went somewhat beyond the FBA). Similar effects have also been observed in Ar [2] and, to some extent, in Ne [3]. In addition, it was found that the dipole limit was approached differently at various electrons ejection angles despite the fact that the amount of momentum transferred from the projectile to the target remained constant. This means that in the case of double ionization the optical limit depends not only on the incident energy and the amount of momentum transfer, as is the case for single ionization, but it also depends on the emission direction of the slow ejected electrons (see [11]). These deviations are seen to be energy dependent and are expected to become larger at lower incident energy in which case the optical limit is increasingly violated. We have therefore performed new low-impact-energy experiments ($\sim$1 keV) in a similar scattering geometry to the work reported in [5] at 5.5 keV. The goal is to address the origin of the deviations between the experiments and FBA-type calculations. To this end, our data will be compared with results from three standard theoretical models, which have been shown to be successful for the description of single-ionization processes or photo-double-ionization processes. Two of these models utilize the FBA in a sense described above. This approximation reduces the four-body problem (three electrons in the field of a residual ion) to a three-body one (the two slow electrons in the residual-ion field). The latter problem is then approached within the framework of the three Coulomb wave method (3C) [12] or using the convergent close-coupling (CCC) formalism [13]. Alternatively, the third model employs a correlated four-body final state (C4FS) as described in [5] and references therein and goes beyond the FBA via the introduction of effective charges. However, as noted in [6], the variation of the effective charges is small, and the non-first Born effects due to this model should be weak.

Throughout this paper, the same notation as in [5] are used. In particular, positive scattering and ejection angles are counted counter-clockwise, starting at the incident beam direction.

2. Experimental

2.1. Experimental procedure

The experimental set-up and procedure have been described extensively elsewhere [2, 6, 14]. Briefly, a coplanar arrangement is used where the incident and the three outgoing electrons lie

in the same plane. The impact energy is $E_0 = 1099$ eV. The scattered electron is observed at a fixed angle, $\theta_a = +1.10^\circ$, with an energy $E_a = 1000$ eV (corresponding to a fixed momentum transfer, $K = 0.45$ au, in the direction $\theta_K = -21.6^\circ$). The value of the scattering angle is measured with an accuracy of $\pm 0.02^\circ$, whereas the spectrometer acceptance angle is $\Delta\theta_a = \pm 0.10^\circ$, which corresponds to a high momentum transfer resolution $\Delta K < \pm 0.006$ au, and a small uncertainty in the momentum transfer direction, $< \pm 0.9^\circ$. The two ejected electrons have identical energies, $E_b = E_c = 10$ eV. They are selected in two opposite half-planes with respect to the electron beam in a double toroidal electrostatic analyser. The angular information contained in the collision plane ($\boldsymbol{k}_0$, $\boldsymbol{k}_a$), i.e. the ejection angles θ_b and θ_c, is preserved upon arrival on the position sensitive detectors. Therefore, multi-angle collection of the ejected electrons is realized over the useful angular ranges $20^\circ < \theta_b < 160^\circ$ and $200^\circ < \theta_c < 340^\circ$. The energy and angle resolutions for the ejected electrons are fixed in the off-line analysis [14] to $\Delta E_b = \Delta E_c = \pm 2$ eV, and $\Delta\theta_b = \Delta\theta_c = \pm 8^\circ$. As far as the present paper is concerned, the data have been sorted into three modes: (i) the so-called 'fixed ejected angle mode' where the escape direction θ_b or θ_c of one electron is fixed and the other one is mapped onto the opposite half-plane; (ii) the 'fixed mutual angle mode' at fixed $\theta_{bc} = (\boldsymbol{k}_b, \boldsymbol{k}_c)$ but varying θ_b or θ_c; and (iii) 'the symmetric geometry mode' where both electrons emerge with equal but opposite angle with respect to the incident beam, $\theta_b = -\theta_c$. A fourth mode, the so-called 'summed mutual angle mode' with varying θ_{bc} but summing over all individual directions θ_b or θ_c which lead to the same θ_{bc}, has been discussed in [11] and will not be repeated here.

The long accumulation time needed to achieve a reasonable statistical error (~ 32 days of continuous, non-stop acquisition for all the data presented in this paper) resulted in a fatigue effect on the detectors, which was corrected as explained in [2, 3, 6, 14] by daily recording 'reference' (e, 2e) distributions. These distributions were also used as an angular calibration of the toroidal analysers by comparing the measured (e, 2e) spectra with well established theoretical ones such as the orthogonalized Coulomb wave (OCW) calculations or the convergent close-coupling calculations. After these corrections (which amount to less than 10–15%), all the angular distributions presented in this paper are obtained on the *same* relative scale. The accuracy of this internormalization is estimated to be significantly better than 10%. In this work, the main emphasis is on the accurate determination of the shape of the distributions to be compared with the different theoretical models. Therefore, no attempt was made to determine the absolute scale for the measured cross sections.

Finally, it should be emphasized that, as discussed in [6], the finite angular and energy resolutions used in this work are not expected to have a severe effect on the measured (e, 2e) or (e, 3e) distributions since it is unlikely that these distributions will have to exhibit any sharp structures.

2.2. Results

The calculated and measured 5DCS are shown in figures 1(a)–(v) and in figures 2(a)–(f) according to the 'fixed ejected angle mode', that is as angular distributions of one electron for fixed emission direction of the second one. In these plots and in the following discussion, we denote by θ_{fix} and θ_{var} the fixed and the variable electron angles, respectively. Figures 3(a)–(c) corresponds to the so-called 'fixed mutual angle mode', that is with variable θ_b and θ_c angles while keeping the mutual angle θ_{cb} fixed. Finally, figure 4 presents the so-called symmetric geometry where both electrons emerge at equal angles on both sides of the incident beam, $\theta_b = -\theta_c$. The fast electron is observed at an angle $\theta_a = +1.10^\circ$, not shown in the figures, hence the $+\boldsymbol{K}$ direction at $\theta_K = -21.6^\circ$ as indicated in figure 1(a).

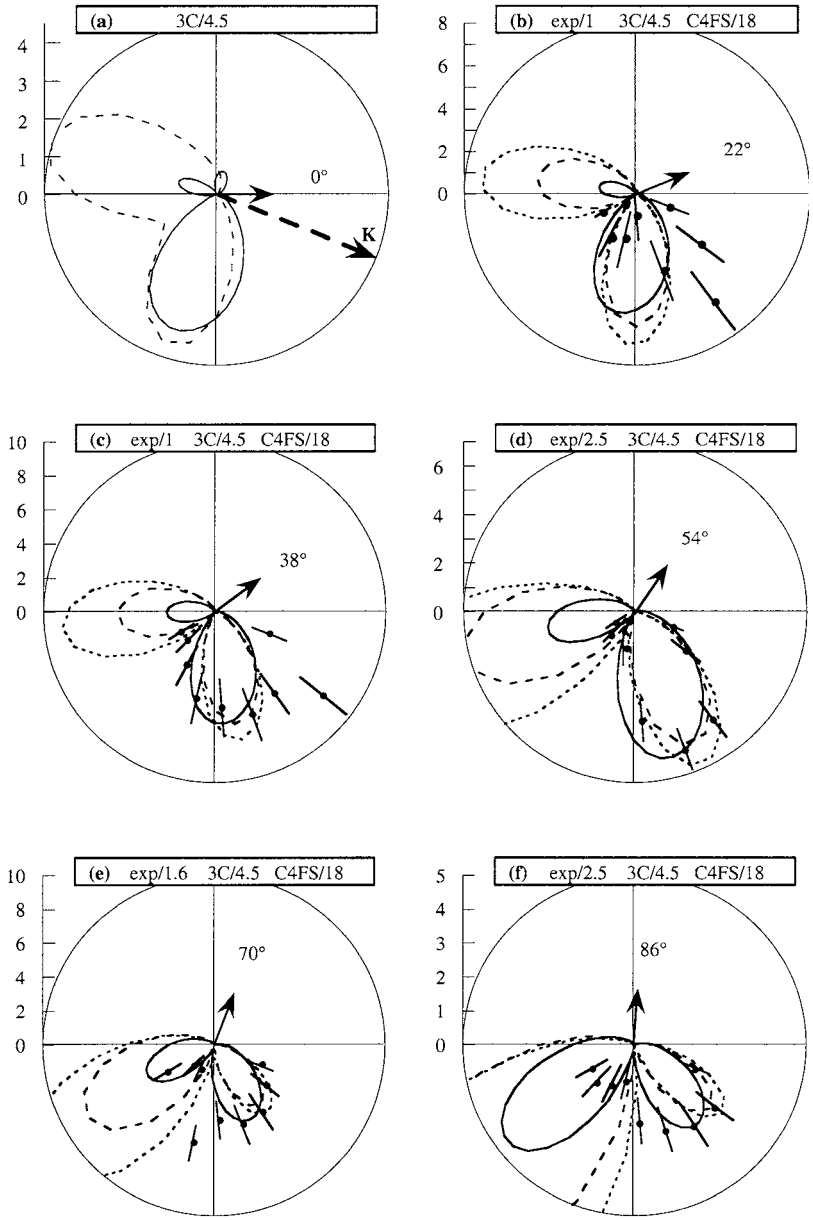

Figure 1. (e, 3e) fivefold differential cross sections (5DCS) for coplanar double ionization of helium at an impact energy $E_0 = 1099$ eV, momentum transfer $K = 0.45$ au ($\theta_a = 1.1°$), and equal ejected energies $E_b = E_c = 10$ eV. The momentum transfer direction is indicated by the bold arrow in panel (*a*). One electron is detected at a fixed angle, θ_{fix}, shown by the thin arrow and the labelling, while the second electron is mapped in the plane. Experiments are shown as full circles, and the error bars represent one standard deviation statistical error. Full curve, CCC results; broken curve, 3C results; dotted curve, C4FS results with a Hylleraas initial-state wavefunction, except in (*k*) and (*v*) where a Slater wavefunction is used. The experimental data are obtained on the same relative scale, but for the sake of clarity they are normalized to the CCC results using different scaling factors, as indicated on each diagram. The absolute scale shown is the CCC one, and is given in 10^{-4} au. Similarly, the 3C and C4FS results are renormalized to the CCC ones, also using different scaling factors, as indicated on each diagram.

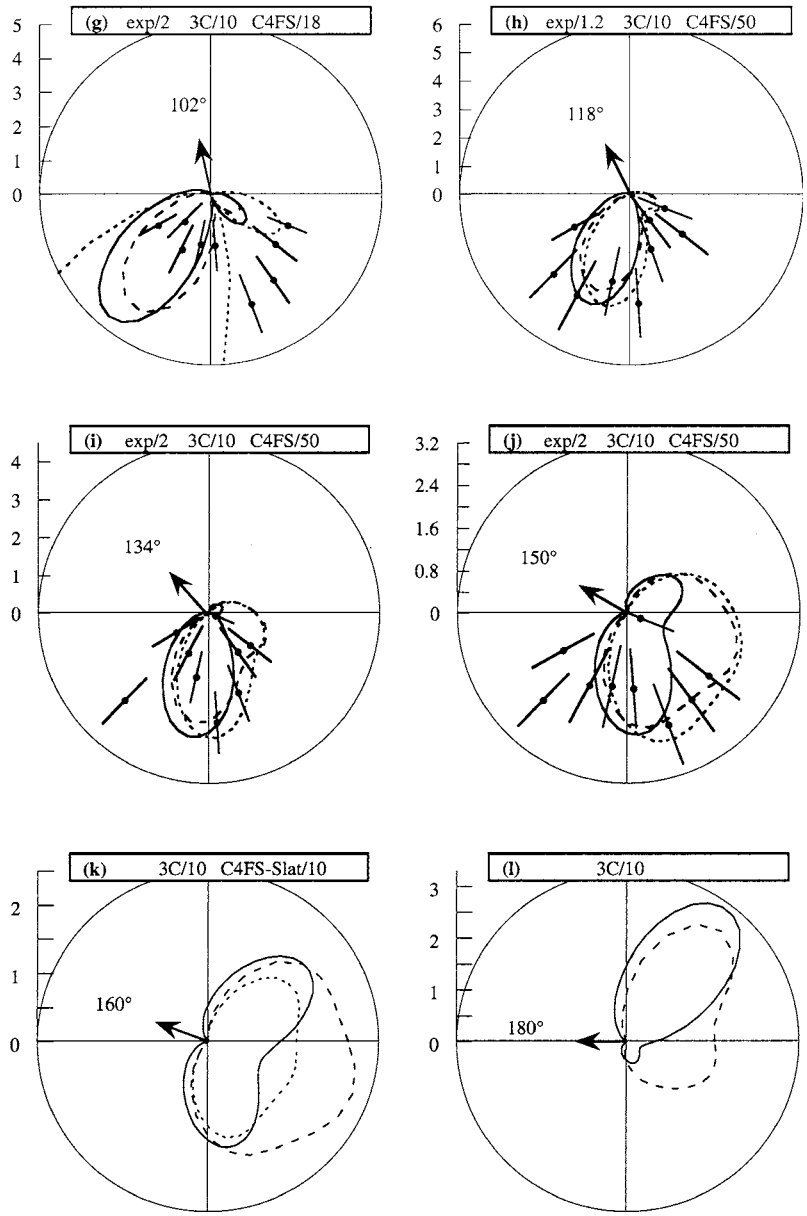

Figure 1. Continued.

Since the data are only relative, we arbitrarily choose to plot all the results by renormalizing them to the absolute scale given by the CCC results. In doing so, and for the sake of clarity of the figures, we have used different scaling factors between experiment and CCC. Similarly, though the 3C and the C4FS results are of course absolute, we have chosen to plot them after a rough renormalization to the CCC ones, as indicated in the figures, in order to put the emphasis on the shape comparison. (This choice is arbitrary and is not meant to favour one model over the others.) However, we recall that the experimental data are obtained on

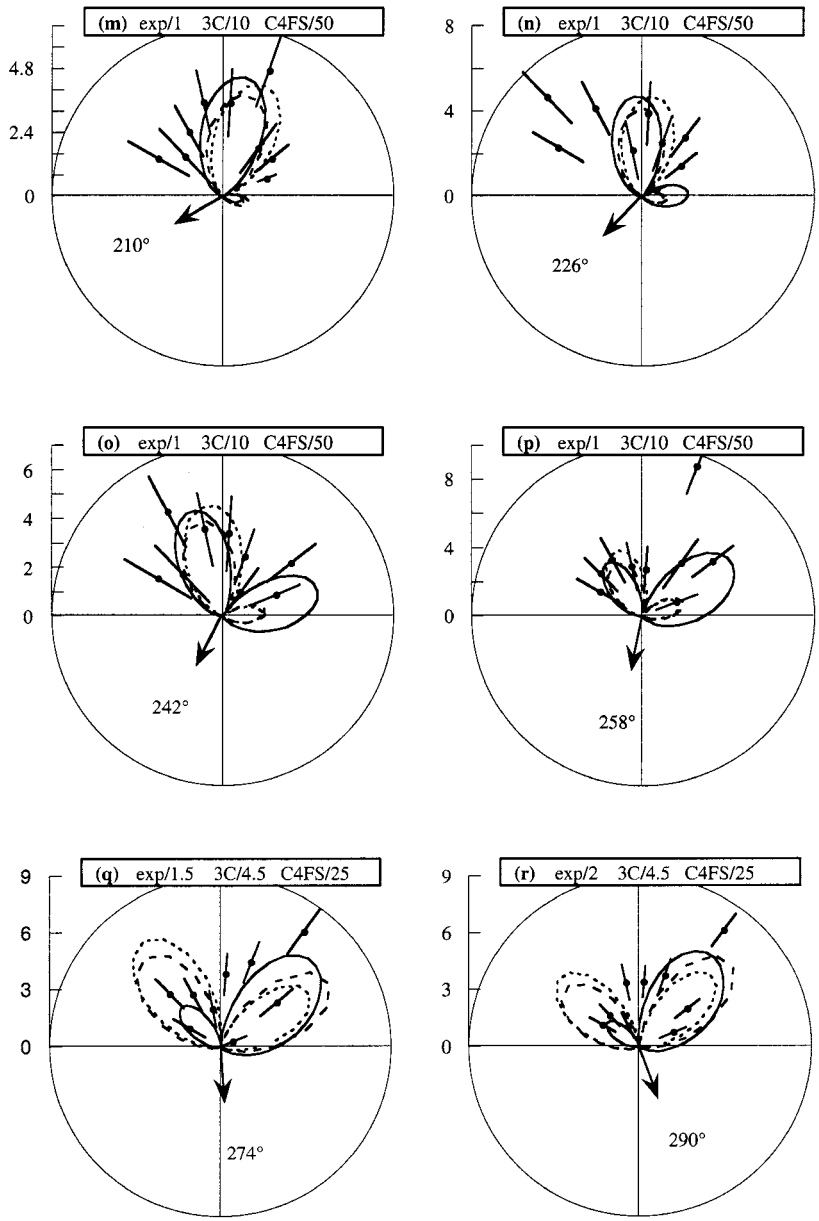

Figure 1. Continued.

the *same* relative scale to within $<10\%$. Therefore, the internal change in the scaling factor between the experiment and each theoretical model is a measure of the ability (or inability) of this model to reproduce the relative scale of the data, whereas its variation from one model to another is a measure of the consistency of the theoretical models in reproducing the absolute scale.

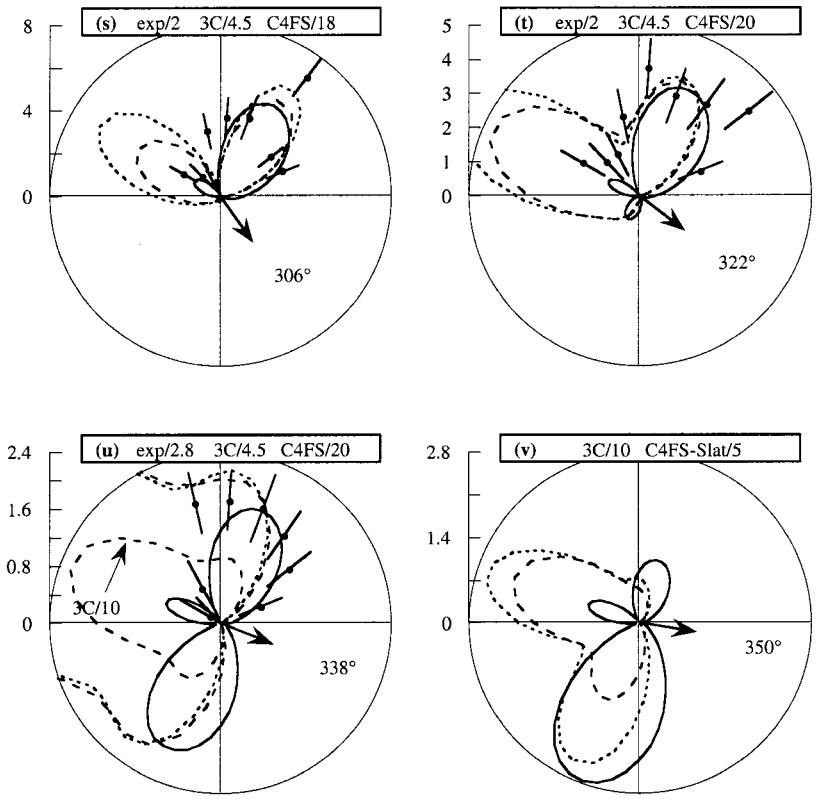

Figure 1. Continued.

2.2.1. Fixed ejected angle mode. As a first observation from figure 1, one may compare the three theoretical results. They generally all yield a two-lobe structure for the 5DCS angular distributions. The two lobes are separated on the one hand by a strict zero intensity for the parallel emission (see, however, the discussion below of figure 3(*c*)), due to the Coulomb repulsion between two electrons with equal energies emerging in the same direction, and on the other hand, by a deep minimum of intensity for the antiparallel or back-to-back emission. This minimum is reminiscent of the node observed in PDI where the back-to-back emission is forbidden, due to the electron pair final-state symmetry [15]. The origin of the dips and maxima in the (e, 3e) cross section and the connection to their PDI counterparts have been explored in [5].

Noticeable exceptions to the two-lobe structure are:

(a) on the one hand, cases (*a*), (*t*), (*u*) and (*v*) corresponding to the fixed electron being emitted forward with respect to the momentum transfer vector, $\boldsymbol{K}$. Here, a third intensity maximum appears roughly in the direction opposite to the fixed electron direction. This maximum appears as a distinct, small lobe in the CCC results and a much wider structure in the 3C and C4FS results. As the back-to-back emission of the two photoelectrons is forbidden in the PDI process, the finite (e, 3e) intensity in this back-to-back configuration must be attributed to non-dipolar contributions. As discussed in [16], within the FBA, only even-parity multipoles of the Born operator contribute to the back-to-back emission.

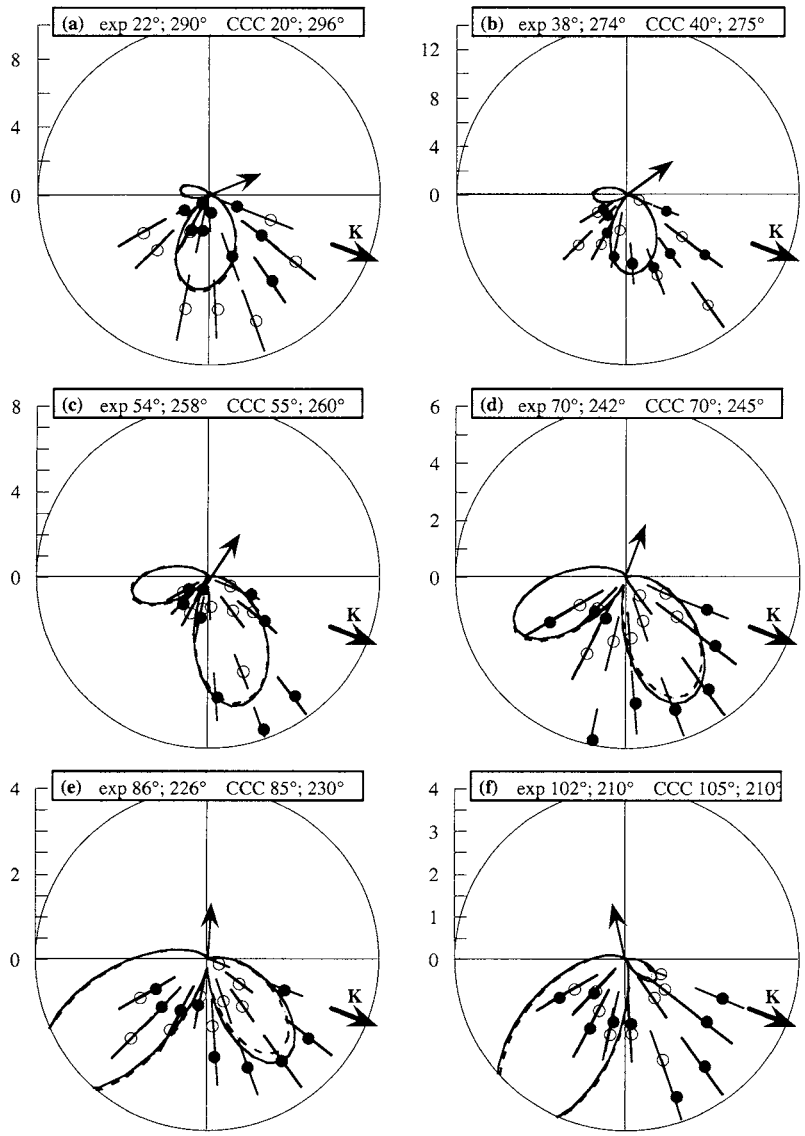

Figure 2. As for figure 1, (e, 3e) 5DCS at $E_b = E_c = 10$ eV. The experimental data and the CCC results obtained at two θ_{fix} angles which are symmetrical with respect to $\boldsymbol{K}$ direction are here superimposed ($\theta_{fix} < 180°$, full circles and full curve; $\theta_{fix} > 180°$, open circles and broken curve). As in figure 1, the CCC absolute scale is used. For the scaling, the experimental data have been divided by the following factors, respectively, from (*a*) to (*f*) 1; 1; 2; 1.6; 2.5; 2.

To see this directly we write the (e, 3e) transition amplitude in the form:

$$T_{(e,3e)} \propto \langle \Psi_{\boldsymbol{k}_b,\boldsymbol{k}_c}(r_b, r_c)\, |\cos(\boldsymbol{K}\cdot\boldsymbol{r}_b) + \cos(\boldsymbol{K}\cdot\boldsymbol{r}_c)|\, \Phi(r_b, r_c)\rangle$$
$$+ i\langle \Psi_{\boldsymbol{k}_b,\boldsymbol{k}_c}(r_b, r_c)\, |\sin(\boldsymbol{K}\cdot\boldsymbol{r}_b) + \sin(\boldsymbol{K}\cdot\boldsymbol{r}_c)|\, \Phi(r_b, r_c)\rangle \quad (1)$$

where $\Psi_{\boldsymbol{k}_b,\boldsymbol{k}_c}(r_b, r_c)$ and $\Phi(r_b, r_c)$ are the wavefunctions of the two slow electrons in the final and initial state, respectively. In general, the final-state wavefunction does not possess a defined parity. However, in the case $\boldsymbol{k}_c = -\boldsymbol{k}_b$ (i.e. in the back-to-back configuration)

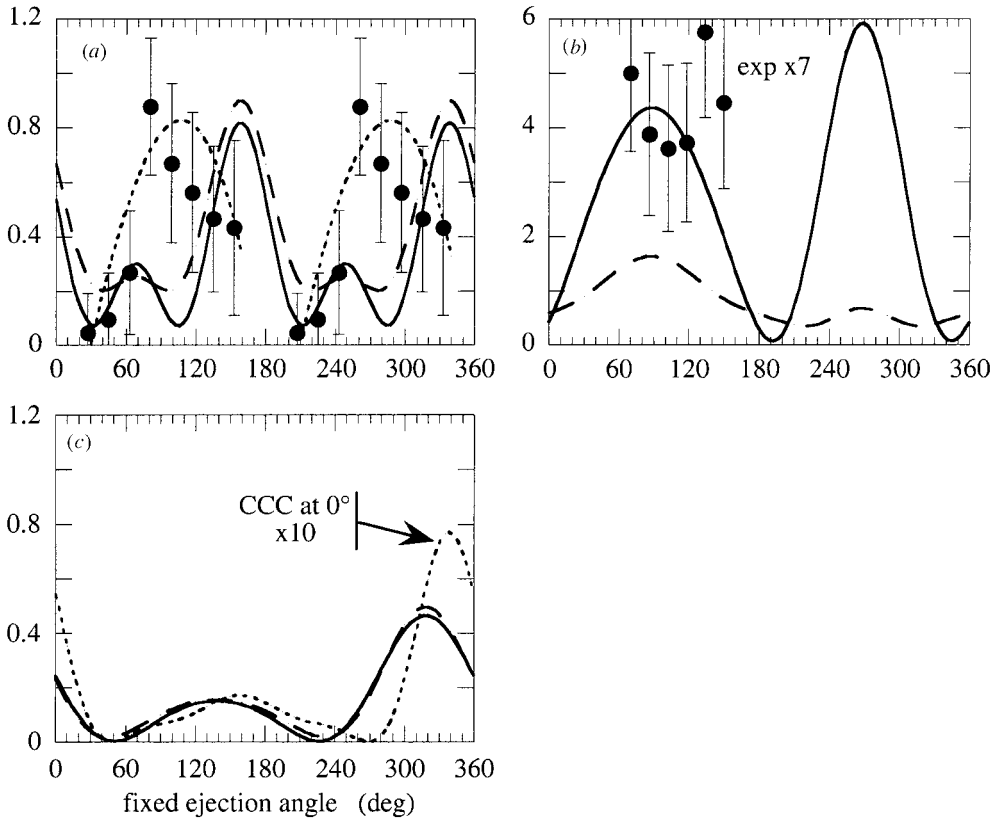

Figure 3. (e, 3e) cross sections in the fixed mutual angle mode, θ_{bc} (see text). Full circles, experiments; full curve, CCC results; broken curve, 3C results divided by 25 in (*a*) and (*b*) and multiplied by 4 in (*c*). (*a*) $\theta_{bc} = 180^\circ$, and the dotted curve is a polynomial fit to the experimental data used to guide the eyes; (*b*) $\theta_{bc} = 140^\circ$; (*c*) $\theta_{bc} = 40^\circ$, and in addition the dotted curve represents the CCC results at $\theta_{bc} = 0^\circ$ magnified by 10. Experimental results are normalized to CCC by multiplying them by 1 in (*a*) and by 7 in (*b*). Kinematical parameters as in figure 1.

$\Psi_{k_b,k_c}(r_b, r_c)$ has an even parity. This follows directly and in an exact manner from the structure of the Schrödinger equation that dictates:

$$\Psi_{k_b,k_c}(r_b, r_c) = \tfrac{1}{2}\left[\Psi_{k_b,k_c}(r_b, r_c) + \Psi_{-k_b,-k_c}(-r_b, -r_c)\right].$$

Therefore, only the cosine term in expression (1) for $T_{(e,3e)}$ contributes in the back-to-back emission case.

(b) Cases (*j*), (*k*), (*l*) and to some extent case (*i*) corresponding to the fixed electron being emitted backward with respect to the $\boldsymbol{K}$ vector. Here, a strong filling of the minimum corresponding to the back-to-back emission is observed, though it is less strong in the CCC than in the C4FS results. This is again clear evidence of non-dipolar contributions which even dominate the dipole term. Or more precisely, as discussed above, the filling of the back-to back emission node in PDI is due to first term in equation (1), i.e. to the odd part of the transition operator. The three theoretical models shown here do not predict the same relative importance for these non-dipole terms. Such effects are appreciably larger than those reported at 5.5 keV impact energy in [6, 11], as is expected due to the lower incident energy and to the larger momentum transfer employed in this paper.

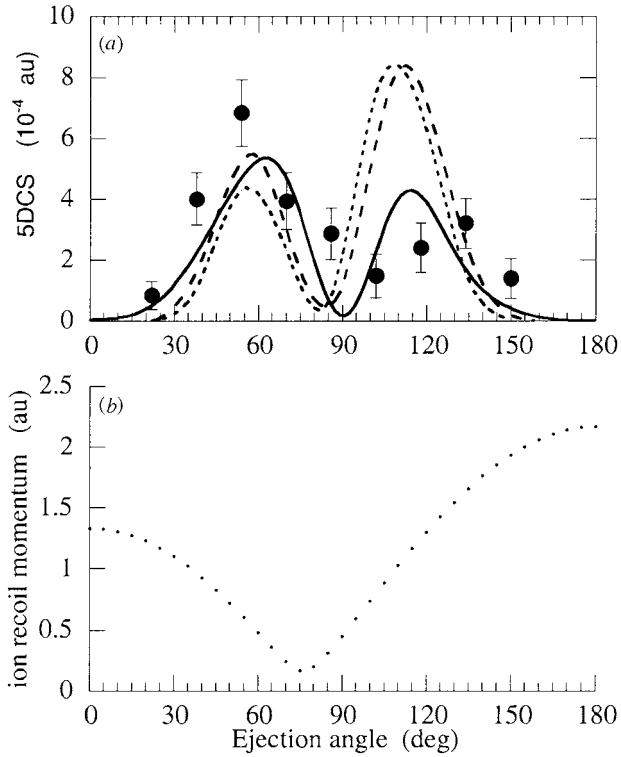

Figure 4. (*a*) (e, 3e) cross sections in the symmetric geometry mode, $\theta_b = -\theta_c$ (see text). Full circles, experiments; full curve, CCC results; broken curve, 3C results divided by 4.5; dotted curve, C4FS results divided by 25. Kinematical parameters as in figure 1. (*b*) the corresponding ion recoil momentum as a function of θ_b.

(c) Apart from these cases where the fixed electron is observed backward or forward in the vicinity of the incident beam direction, the three theories predict a small probability for the back-to-back emission in agreement with the PDI expectation, meaning that here the optical limit is closely approached. All observation (a)–(c) confirm the conclusion made in [5, 11] that the dipolar limit is reached differently depending on the directions of the momentum vectors $\boldsymbol{k}_b$ and $\boldsymbol{k}_c$, even though the momentum transfer, the incident energy and the outgoing electron energies are kept fixed.

Now let us have a closer look at the shape of the theoretical distributions in figure 1. The intensity ratio of the two lobes, when present, is quite different from one model to another. For instance, CCC calculations predict one large and one small lobe in case (*b*) where $\theta_{fix} = 22^\circ$, while both C4FS and 3C calculations yield two almost identical lobes. The situation is practically reversed in case (*o*) where $\theta_{fix} = 242^\circ$, with two identical lobes for CCC and very asymmetric lobes for C4FS and 3C. Generally speaking, the distributions obtained with the C4FS and 3C models are very close to each other as to the shape, and are significantly different from the CCC ones. This can be explained by the way the final-state wavefunction is calculated in different models. The C4FS and 3C final-state wavefunctions are most accurate at the asymptotic region of large distances from the nucleus. In contrast, the CCC final-state wavefunction is accurate at a short range from the nucleus and loses its accuracy in the asymptotic region. Nevertheless, the CCC calculations with the same final-state

wavefunction provide reliable absolute cross sections for the related PDI process. In addition, the prediction of the CCC model agrees as to the shape with recent (e, 3e) measurements obtained on a *relative scale* by Dorn *et al* [17] for a similar kinematics of a large incident energy and a small momentum transfer.

Another observation concerns the relative magnitude of the cross sections given by the three models. With the normalization procedure explained above, one sees that there is a factor of 10 difference in magnitude between CCC and 3C results in cases (g)–(p), 3C yielding larger cross sections. This factor reduces to 4.5 in the other cases. We note that cases (g)–(p) correspond to the fixed electron being observed in the 'backward half-plane' (with respect to the incident direction), that is $90^\circ < \theta_{\rm fix} < 270^\circ$, while the other cases correspond to the fixed electron being observed in the 'forward half-plane', that is $-90^\circ < \theta_{\rm fix} < 90^\circ$. Similarly, the C4FS results are a factor of 10–50 larger than the CCC ones depending on the $\theta_{\rm fix}$ value, with more or less the same remark applying as to the backward and forward half-planes. On the other hand, the ratio of 3C to C4FS results is almost constant, C4FS yielding about ~ 5 times larger cross sections at practically all $\theta_{\rm fix}$ values. Therefore, as noted above concerning the shapes, the C4FS and 3C models yield comparable results but both deviate significantly from the CCC calculations. Part of these deviations may have their origin in the following observation: the C4FS results presented here make use of a three-term Hylleraas-type ground state description of the He atom. Calculations within the same model have also been performed using a poorer description of the initial state, namely a Slater-type wavefunction. The results (not presented here) are very similar in shape to the Hylleraas ones, but differ in magnitude being a factor of ~ 6 larger, the use of yet another choice of initial-state wavefunction leads basically to the same shape for the angular patterns but alters the absolute value of the cross sections significantly. This may be taken as a good illustration of the sensitivity of the C4FS results to the initial-state description. The 3C calculations utilize a six-term Hylleraas type ground state wavefunction [18], which gives a good value for the energy of the ground state ($E = -2.903\,115$ au). The CCC calculations are performed with the more elaborate 20-term Hylleraas wavefunction. CCC calculations in the velocity gauge of the Born operator, not shown here, have also been performed with an 18-term MCHF expansion. They yield very similar results, proving the stability of the CCC calculation to the ground state wavefunction when a large basis set is used. Therefore, it is likely that at least part of the difference in absolute scale between the three theories has its origin in the quality of the ground state wavefunction. However, a clear-cut answer to this point would necessitate a direct comparison of several initial-state wavefunctions of different quality using the *same* final-state description, that is for *each* of the three theoretical models.

In general, all three models do grossly reproduce the shape of the experimental 5DCS distributions of figure 1 within the uncertainty given by the error bars of the experiments and by the fact that the data are only recorded in one half-plane. Nonetheless, there are obvious substantial deviations between theories and experiment.

(a) First, none of the considered models correctly reproduces the relative scale of the experimental data. In addition, there is also no internal consistency in the relative scale between the different theoretical results. If cases (b) and (c) are taken as a reference where the normalization constant between experiment and each theory is arbitrarily given a value equal to 1, then it can easily be inferred from figure 1 that it would be necessary to divide the experiment by a variable factor which takes values between 0.35 and 2.8 in order to bring the measured data in cases (d)–(u) into reasonable agreement with the calculated results. Such a large variable factor is much greater than the estimated

$<10\%$ accuracy of the relative scale on which the measured cross sections are brought. Besides, from the numerous tests performed, in particular by measuring known (e, 2e) angular distributions, it is extremely unlikely that such a variable factor might be due to an experimental fault.

(b) In a number of cases, e.g. (*d*), (*h*) and (*o*), the angular position of the calculated lobes is in a nice agreement with the measured ones, whereas for several other cases, e.g. (*b*), (*g*), (*n*) and (*q*) large shifts are observed, which may amount up to some 45°. In this respect, the C4FS and 3C models yield identical positions of the lobes, whereas the main lobe in the CCC model generally appears to be rotated backwards by $\sim 10^\circ$ with respect to the other models.

(c) Cases (*u*) and (*k*) are of particular interest since the fixed electron is observed along $+\boldsymbol{K}$ or (approximately) along $-\boldsymbol{K}$, respectively. Under these conditions, it was shown [19] that any first-order model must yield a symmetrical distribution about $\pm\boldsymbol{K}$. This is the case for all three models, including the C4FS which goes beyond FBA through the introduction of effective charges. This either means that the non-first-order effects are intrinsically small under these geometries, or, as previously noted in [6,8] that their contribution to the C4FS cross sections is small. Unfortunately, the limited range of the experimental data does not allow a conclusion concerning a possible breaking of symmetry being reached. It is also interesting to note that the three models predict a strong (CCC) or very strong (C4FS and 3C) relative contribution of the back-to-back emission under this geometry (this contribution is, in fact, maximum there, see figure 3(*a*)). This appears to be in conflict with the experimental observation in case (*u*) where the measured back-to-back intensity approaches zero.

(d) As noted in [6, 11], the PDI cross sections distributions obtained for two electrons fixed angles which are symmetrical with respect to the electric field direction ϵ must be mirror images of each other with respect to this ϵ direction. In the electron impact case, $\boldsymbol{K}$ plays the role of the ϵ direction in the dipole limit. Therefore, we exploit this mirror symmetry in figure 2 in which some of the data of figure 1 are accordingly superimposed on each other. Comparison is made with the CCC results obtained under the same transformation. We see clearly from figure 2 that this symmetry transformation does not produce much change in the CCC results which are thus quite close to the dipole limit. On the other hand, even considering the large error bars, the experimental data *are not* invariant under such a transformation. This might show how important are the deviations from the optical limit, but it might also indicate the large role played by non-first Born processes, even though the incident energy is large (1.1 keV) and the momentum transfer is small (0.45 au). A similar observation was made in [6], but in general the deviations from 'perfect' symmetry were smaller, as one would expect from the higher incident energy (5.5 keV) and smaller momentum transfer (0.24 au) used in [6].

2.2.2. Fixed mutual angle mode. Figure 3 presents angular distributions in the so-called fixed mutual angle mode, that is with variable θ_b and θ_c angles while keeping the mutual angle θ_{bc} fixed. The experiments are compared with the CCC and the 3C results (C4FS results are almost identical to the 3C ones except for the magnitude). In figures 3(*a*) and (*b*) the two ejected electrons emerge at a large angle from each other, whereas in figure 3(*c*) they asymptotically fly out close to each other which enhances the final-state Coulomb repulsion between them. In all cases the two models do not produce the same magnitude of cross sections as discussed above, hence different normalization factors are used (as indicated in the figures) in order to put the emphasis on the shape comparison.

- Case (*a*) with a mutual angle $\theta_{bc} = \pi$ is a very interesting one since it corresponds to the forbidden back-to-back emission in PDI (i.e. in PDI this graph would be strictly zero everywhere). In other words, this graph represents a *direct measure* of the non-dipolar effects involved in the present (e, 3e) process, in the sense discussed following equation (1). As noted above, theories predict that these non-dipolar effects are maximum when the pair of electrons is ejected along $\pm\boldsymbol{K}$, whereas the maximum probability in the experiments occurs when the electron-pair axis is rotated by $\sim 60^\circ$ from this direction. Moreover, the two first-order theories show the expected symmetry about the $\pm K$ direction (at 338° and 158°, respectively) whereas the experiment does not. Both the angular shift and the breaking of symmetry may be directly attributed to second- or higher-order effects in the projectile–target interaction process.
- In figure 3(*b*), both theories show two lobes but with different intensity distributions. Though limited in their extent, the data seem to indicate a minimum at 90–100° where both calculations show a maximum.
- In figure 3(*c*), though no data could be measured, it is interesting to compare the result of the two calculations. At 40° mutual angle both models yield almost indistinguishable angular distributions as to the shape. However, in contrast with all the above observations, the CCC cross sections are now a factor of four *larger* than the 3C ones. This might be explained in the 0° behaviour of the CCC. Indeed, at 0° mutual angle the 3C model (and the C4FS model) yield a vanishing cross section as expected from the Coulomb repulsion which forbids the two ejected electrons to emerge in the same direction with the same velocity. In contrast, the CCC model fails to strictly fulfil this selection rule as it predicts a non-zero intensity. However, the corresponding cross sections are small, about two orders of magnitude smaller than a typical CCC lobe intensity in figure 1, and roughly one order of magnitude smaller than the 'DPI-forbidden' intensities involved in figure 3(*a*).

2.2.3. Symmetric geometry. In figure 4, the data have been sorted for the two ejected electrons to emerge at equal but opposite angles, $\theta_b = -\theta_c$. In (e, 2e) processes, such a symmetric geometry is well known to be very sensitive at large angles to second-order effects [20], and this has allowed the identification of the observed (e, 2e) large-angle peak [21,22] as being due to a double mechanism involving a backward elastic scattering of the projectile followed by a binary e–e collision. In this representation, the present theoretical and experimental results show two peaks, one forward at about 60° and one backward at $\sim$130° in the experiment and $\sim$110° in the theories. The experiment shows a backward-to-forward peak ratio of ~ 0.5. The CCC ratio of ~ 0.8 is close to the measurements, whereas the other two theories show ratios larger than 1, roughly 1.5. In the lower panel of the figure we plot the corresponding magnitude of the ion recoil momentum, k_{ion}. Comparing the upper and the lower panels of the figure, a striking similarity is observed as to the position of the minimum (especially with the theoretical minimum) at $\theta_b \sim 80^\circ$. When k_{ion} is minimum, the Bethe sphere is closely approached (the Bethe sphere is reached when the momentum transfer $\boldsymbol{K}$ is fully absorbed by the pair of ejected electrons, the ion remaining spectator, i.e. $k_{ion} = 0$). It has been argued [16] that under these kinematical conditions the cross section should be maximal, while it is observed here to be minimal. This apparent contradiction was also noted in [5] and was attributed to the fact that under the present near-dipole conditions, the optical transition is forbidden for two 'free' electrons which is the condition for the Bethe sphere. The fact that the experimental minimum occurs at a larger angle than in the calculations might be due to the non-dipole contributions which are not fully taken into account in the models as suggested above, e.g. in figure 3(*a*).

3. Conclusion

We presented a large body of new experimental data on the (e, 3e) fully resolved cross sections for the double ionization of helium, in the coplanar geometry and under equal energy sharing 10 + 10 eV. The data were compared in different angular modes with the best available first-order theories, namely the 3C, C4FS and CCC models.

The three theories do not predict the same absolute scale for the 5DCS. This could partly be due to the different descriptions of the initial state used, from poor to more elaborate. However, when compared with the experiments, they do not predict the correct relative scale for different angular distributions neither. Given that the CCC describes the PDI cross sections so well, its present failure to reproduce the relative scale clearly illustrates a somewhat different nature of the PDI and (e, 3e) processes.

The experiments as well as all theories display a strong filling of the node corresponding to the forbidden back-to-back emission in PDI, or even display an additional lobe at this position. This behaviour obviously reflects a strong manifestation of non-dipolar effects in the projectile–target interaction which become prominent when the fixed electron is emitted either forward or backward around the momentum transfer direction. However, the three theoretical models do not predict the same relative importance for these effects. Such effects are appreciably larger than those observed at 5.5 keV, as is expected from the lower impact energy and larger momentum transfer of this work. Moreover, these effects do vary appreciably with the emission directions, which confirms our earlier conclusion [5, 11] that the dipolar limit is reached differently depending on the orientation of the $\boldsymbol{k}_{\rm b}$ and $\boldsymbol{k}_{\rm c}$ vectors, even though the momentum transfer, the incident energy and the outgoing energies are kept fixed. A similar experiment at much higher incident energy, 10 keV or more, is highly desirable in order to probe when and how the optical limit is reached.

On the other hand, while the CCC theory almost fulfils the 'mirror symmetry' when superimposing angular distributions taken at symmetrical $\theta_{\rm fix}$ angles with respect to $\boldsymbol{K}$, the experiments do not. This might indicate the large role played by non-first Born processes. Another indication of the importance of these effects is found when the pair of electrons is detected back-to-back while rotating the e–e axis (figure 3): the three first-order theories show the expected symmetry about the $\pm\boldsymbol{K}$ direction, whereas this symmetry is broken in the experimental data. A similar experiment at lower incident energy is also desirable in order to enhance the observed effects. Such an experiment has recently been performed in our group and is currently under analysis.

Acknowledgments

The authors are grateful to Dr A Huetz for helpful discussions. They also acknowledge the technical assistance and skills of Mr A Abadia. One of the authors (AK) wishes to thank the Université de Paris-Sud XI for a Professeur invité position.

References

[1] Lahmam-Bennani A, Duguet A, Grisogono A M and Lecas M 1992 *J. Phys. B: At. Mol. Opt. Phys.* **25** 2873
[2] El Marji B, Schröter C, Duguet A, Lahmam-Bennani A, Lecas M and Spielberger L 1997 *J. Phys. B: At. Mol. Opt. Phys.* **30** 3677
[3] Schröter C, El Marji B, Lahmam-Bennani A, Duguet A, Lecas M and Spielberger L 1998 *J. Phys. B: At. Mol. Opt. Phys.* **31** 131
[4] Taouil I, Lahmam-Bennani A, Duguet A and Avaldi L 1998 *Phys. Rev. Lett.* **81** 4600
[5] Lahmam-Bennani A, Taouil I, Duguet A, Lecas M, Avaldi L and Berakdar J 1999 *Phys. Rev.* A **59** 3548

[6] Kheifets A, Bray I, Lahmam-Bennani A, Duguet A and Taouil I 1999 *J. Phys. B: At. Mol. Opt. Phys.* **32** 5047
[7] El Mkhanter R and Dal Cappello C 1998 *J. Phys. B: At. Mol. Opt. Phys.* **31** 301
[8] Grin M, Dal Cappello C, El Mkhanter R and Rasch J 2000 *J. Phys. B: At. Mol. Opt. Phys.* **33** 131
[9] Nebdi H 2000 *PhD Thesis* Université Catholique de Louvain
[10] Popov Yu V, Dal Cappello C and Ancarani L U 2001 *Many Particle Spectroscopy of Atoms and Molecules, Clusters and Surfaces* ed J Berakdar and J Kirschner (New York: Plenum, Dordrecht: Kluwer)
[11] Lahmam-Bennani A, Duguet A, Taouil I and Gaboriaud M N 2001 *Many Particle Spectroscopy of Atoms and Molecules, Clusters and Surfaces* ed J Berakdar and J Kirschner (New York: Plenum, Dordrecht: Kluwer)
[12] Joulakian B, Dal Cappello C and Brauner M 1992 *J. Phys. B: At. Mol. Opt. Phys.* **25** 2863–71
[13] Kheifets A S and Bray I 1998 *Phys. Rev.* A **58** 4501
[14] Duguet A, Lahmam-Bennani A, Lecas M and El Marji B 1998 *Rev. Sci. Instrum.* **69** 3524
[15] Huetz A, Selles P, Waymel D and Mazeau J 1991 *J. Phys. B: At. Mol. Opt. Phys.* **24** 1917
[16] Berakdar J and Klar H 1993 *J. Phys. B: At. Mol. Opt. Phys.* **26** 4219
[17] Dorn A, Kheifets A S, Schröter C D, Najjari B, Höhr C, Moshammer R and Ullrich J 2001 *Phys. Rev. Lett.* **86** 3755
[18] Joulakian B and Dal Cappello C 1993 *Phys. Rev.* A **47** 3788
[19] Dal Cappello C and Le Rouzo H 1991 *Phys. Rev.* A **43** 1395
[20] Byron F W Jr and Joachain C J 1989 *Phys. Rep.* **179** 211
[21] Pochat A, Tweed R J, Peresse J, Joachain C J, Piraux B and Byron F W 1983 *J. Phys. B: At. Mol. Phys.* **16** L775
[22] Rösel T, Dupré C, Röder J, Duguet A, Jung K, Lahmam-Bennani A and Ehrhardt H 1991 *J. Phys. B: At. Mol. Opt. Phys.* **24** 3059